ARTICLE

Cystine supplementation rebalances the redox homeostasis of microenvironment in non-small cell lung cancer cells and reverses their resistance to docetaxel

Si-jia Li[1], Bei Cao[2], Zhen-yao Lu[1], Run-bin Sun[1,2], Su-han Guo[1], Yuan Xie[1], Ji-ye Aa[1] and Guang-ji Wang[1]

Continuous docetaxel (DTX) treatment of non-small cell lung cancer induces development of drug resistance, but the mechanism is poorly understood. In this study we performed metabolomics analysis to characterize the metabolic patterns of sensitive and resistant A549 non-small cell lung cancer cells (A549/DTX cells). We showed that the sensitive and resistant A549 cells exhibited distinct metabolic phenotypes: the resistant cells were characterized by an altered microenvironment of redox homeostasis with reduced glutathione and elevated reactive oxygen species (ROS). DTX induction reprogrammed the metabolic phenotype of the sensitive cells, which acquired a phenotype similar to that of the resistant cells: it reduced cystine influx, inhibited glutathione biosynthesis, increased ROS and decreased glutathione/glutathione disulfide (GSH/GSSG); the genes involved in glutathione biosynthesis were dramatically depressed. Addition of the ROS-inducing agent Rosup (25, 50 μg/mL) significantly increased P-glycoprotein expression and reduced intracellular DTX in the sensitive A549 cells, which ultimately acquired a phenotype similar to that of the resistant cells. Supplementation of cystine (1.0 mM) significantly increased GSH synthesis, rebalanced the redox homeostasis of A549/DTX cells, and reversed DTX-induced upregulation of P-glycoprotein, and it markedly improved the effects of DTX and inhibited the growth of A549/DTX in vitro and in vivo. These results suggest that microenvironmental redox homeostasis plays a key role in the acquired resistance of A549 cancer cells to DTX. The enhancement of GSH synthesis by supplementary cystine is a promising strategy to reverse the resistance of tumor cells and has potential for translation in the clinic.

Keywords: non-small cell lung cancer cells; docetaxel; drug resistance; metabolomics; microenvironment; redox homeostasis; P-glycoprotein; cystine; Rosup; NAC

INTRODUCTION

Docetaxel (DTX), a semisynthetic paclitaxel, is a potent agent for the treatment of various tumors [1]. It reversibly binds to free tubulin with high affinity, promotes the assembly of microtubules from tubules and stabilizes microtubules by preventing depolymerization, resulting in cell cycle arrest at the G2/M checkpoint [2]. Clinically, DTX is used mainly for the treatment of locally advanced or metastatic cancer after failure of prior chemotherapy. For example, DTX can be used as a single agent in the treatment of patients with locally advanced or metastatic non-small cell lung cancer (NSCLC) after failure of prior platinum-based chemotherapy [3]. Unfortunately, long-term treatment with DTX usually leads to drug resistance, cancer metastasis and recurrence, which greatly affects the efficacy of chemotherapy and limits the clinical use and prognostic value of DTX [4]. It has been estimated that a significant number of NSCLC patients are not responsive to current chemotherapeutic regimens due to resistance [5]. In vitro, chronic exposure of sensitive A549 lung cancer cells to DTX produces a stable resistant cell line, A549/DTX cells, which are appropriate experimental models for the study of the mechanism of antitumor drug resistance.

In the exploration of the underlying mechanism of DTX-induced chemoresistance, genomics and proteomics have revealed some candidate genes and proteins that are involved in NSCLC drug resistance. In contrast with sensitive lung cancer cells, DTX-resistant cells show increased levels of multidrug resistance genes, such as P-glycoprotein (P-gp) [6–8], multidrug resistance-associated protein 7 [9] and the apoptotic pathway genes survivin and Bcl-2 genes [6]. However, the fundamental biochemical mechanism of acquired resistance in lung cancer cells remains unclear. Considering that, in the process of antitumor drug treatment, tumor cells inevitably undergo adaptive changes to drug exposure and ultimately acquire drug resistance, exploring biochemical changes and the tumor microenvironment may enable us to obtain a better understanding of drug resistance and the underlying initial factor(s) triggering acquired resistance. It has been well documented that tumor cells are highly metabolically flexible and prone to metabolic reprogramming, and extensive metabolic reprogramming of cancer cells has been regarded as the seventh hallmark of tumors [10]. Metabolomics, which allows high-throughput analysis of endogenous compounds, is widely employed in the study of cancer metabolism

Supplementary cystine reverses the resistance of A549 cells
SJ Li et al.

2133

[11, 12]. Based on metabolomics, increasing evidence has shown that endogenous metabolites and metabolic reprogramming play important roles in tumor growth, invasiveness and metastasis development, including glycine [13], glutamine [14], aspartic acid [15], and serine [16, 17]. Comparative studies of the differential effects of chemotherapeutic agents on drug-sensitive and drug-resistant cells may provide useful information for understanding the mechanisms underlying chemoresistance and for discovering new targets for reversing resistance. Consistent with our expectations, a previous study by our team on sensitive and resistant breast cancer cells suggested distinctly different metabolic patterns in the two types of cells [18]. Our results also showed that resistance in MCF-7 breast cancer cells was dependent on the microenvironment of these cells, especially on reactive oxygen species (ROS) and redox homeostasis [19].

However, little is known about the metabolic characteristics of sensitive and resistant lung cancer cells and whether the microenvironment and redox homeostasis are primarily involved in acquired resistance in A549 cells. Moreover, the in vitro to in vivo translatability is unknown. Hence, in the current study, as an attempt to characterize the metabolic pattern of resistant cells and identify potential markers of resistance, we profiled metabolites in A549 and A549/DTX cells and the metabolites in culture medium before and after DTX exposure by using both liquid chromatography quadrupole-time of flight mass spectrometry (LC Q-TOF/MS) and gas chromatography mass spectrometry (GC/MS). The role of redox homeostasis in the sensitization of cells to DTX was further studied both in vivo and in vitro to gain further insight into the mechanism underlying DTX resistance.

MATERIALS AND METHODS
Agents
DTX was commercially available from Selleck (Houston, TX, USA), and DTX injection was commercially available from Hengrui Medicine (Lianyungang, Jiangsu, China). Cystine was commercially available from Sigma-Aldrich (St Louis, MO, USA).

Cell cultivation and harvest
Human NSCLC A549 cells and DTX-resistant A549 cells (A549/DTX cells) were purchased from the Type Culture Collection of the Chinese Academy of Sciences (Shanghai, China). These cell lines were grown in RPMI-1640 medium supplemented with 10% (v/v) fetal bovine serum and 100 U/mL penicillin and streptomycin at 37 °C with 5% carbon dioxide.

Cell viability assay
A549 and A549/DTX cells (5000 cells per well) were cultured in 96-well plates for the cell viability assay. After treatment, cell viability was tested by using the Cell Counting Kit-8 (Beyotime, Shanghai, China) according to the manufacturer's protocol.

Flow cytometry analysis of cell apoptosis
A549 and A549/DTX cells were seeded in 6-well plates evenly. After exposure to DTX or cystine supplementation, the cells were washed twice with cold PBS and resuspended in 1× Binding Buffer. Then the 100 μL of the solution was added and stained with FITC Annexin V and PI (Annexin V FITC Apop Dtec Kit I, BD Biosciences, Franklin Lake, NJ, USA), respectively. Data were acquired on a BD Accuri C6 within 1 h.

Quantitative PCR analysis
Total RNA was extracted from cells and tumors using RNAiso Plus reagent according to the manufacturer's protocol. Reverse transcription of 500 ng of total RNA to evaluate genes in cells was performed using SuperScript II Reverse Transcriptase (Invitrogen, Carlsbad, CA, USA). Quantitative reverse transcription PCR analysis was performed using SYBR green PCR Master Mix and a

MyIQ real-time PCR cycler (Bio-Rad, Hercules, CA, USA), and the expression of the targets was normalized to that of β-actin. The primer sequences are listed in Table S1.

Determination of DTX concentrations in cells and tumors
Cells were collected after incubation with DTX or cysteine supplementation at 37 °C for the indicated time. Subcellular organelles were extracted from the cells with the Mitochondria/Nuclei Isolation Kit (KGA828, KeyGENBioTECH, Nanjing, Jiangsu, China) in accordance with the manufacturer's instructions. The DTX concentration was determined by LC-MS/MS as previously reported [20]. The concentration of DTX in cells or subcellular organelles was normalized to the protein levels in each sample, and the DTX concentration in tumors was normalized to the tumor weight. Protein concentrations were measured using a BCA protein assay kit (Beyotime).

Immunofluorescence assay for P-gp expression
Cells were plated in 6-well plates before harvest. After treatment and washing, the cells were incubated with a PE-conjugated anti-P-gp polyclonal antibody or a negative control for 30 min at 37 °C (PE anti-human CD243 (MDR-1) antibody, BioLegend, San Diego, CA, USA). After washing, the cells were analyzed on a BD Accuri C6 cytometer within 1 h.

Metabolomics assay of cells, medium, plasma and tumor
The GC/MS and LC/Q-TOF MS metabolomics analysis method were performed as reported previously [18, 21]. For the obtained multivariate data, partial least squares discriminant analysis (PLS-DA) was performed using SIMCA-P 13.0 software (Umetrices, Umeå, Sweden) [22, 23]. Metabolomics pathway analysis of the metabolic biomarkers was carried out using MetaboAnalyst (www.metabonalyst.ca) [24].

Intracellular reactive oxygen species measurement
A549 and A549/DTX cells were cultured in 12-well plates. A treatment, the cells were incubated for 30 min with 10 μM 2′,7′-dichloro-hydrofluorescein diacetate (DCFH-DA)(Sigma-Aldrich), harvested and analysed using a microplate reader Powerwave 200 (Bio-Tek Instruments, Winooski, VT, USA) at wavelength of 488/535 nm or flow cytometry on BD Accuri C6. The ROS values were normalized to the protein levels in each sample.

Western blotting
After treatment, cell or tumor membrane proteins were prepared for Western blot analysis as described by the manufacturer of a membrane and cytosol protein extraction kit (Beyotime). Proteins in the membrane extracts were separated by 8% sodium dodecyl sulfate-polyacrylamide gel electrophoresis (SDS-PAGE) and transferred to polyvinylidene fluoride membranes (Bio-Rad). After blocking with 5% BSA, the membranes were incubated overnight with primary antibodies against P-gp (1:1000, ab170904, Abcam, Hercules, CA, USA), SLC7A11 (1:1000, ab37185, Abcam) and Na$^+$/K$^+$ ATPase (1:10000, ab185210, Abcam) at 4 °C, followed by incubation with HRP-labeled goat anti-rabbit IgG (H + L) (Beyotime) for 1 h at 37 °C. The signal was visualized with a BeyoECL Plus kit (Beyotime) and captured with a ChemiDoc XRS + system (Bio-Rad). Band intensity was quantified by Image Lab statistical software (Bio-Rad). Total protein was extracted from cells or tumor tissues with RIPA buffer (Beyotime) and separated by 10% SDS-PAGE. The primary antibodies were anti-GCLC (γ-GCS) (1:1000, ab207777, Abcam) and anti-glutathione synthetase (GSS) (1:1000, ab133592, Abcam).

Intracellular accumulation of rhodamine 123 assay
The Rhodamine 123 (Rho123) (Sigma-Aldrich), a classic fluorescence substrate of P-gp, was monitored for the evaluation of P-gp function. Briefly, A549 cells or A549/DTX cells were plated in 12-

Supplementary cystine reverses the resistance of A549 cells
SJ Li et al.

2134

well or 96-well plates. After treatment and washing, the cells were incubated with Hank's Balanced Salt Solution (HBSS, 37 °C, pH 7.4) containing Rho123 (5 μM) for 1 h. The accumulation was stopped by rinsing the cells with ice-cold HBSS for three times. After collecting cell, the cells were analysed via BD Accuri C6 within 1 h. In a parallel experiment, the intracellular accumulation of Rho123 was detected by Lion Heart (Biotec Instruments).

Animal experiments
Athymic nude male mice (BALB/c-*nu/nu*) aged 4–6 weeks and weighing 18–22 g were purchased from Shanghai Slike Experimental Animals Co. (Shanghai, China) and were used to establish subcutaneous A549 or A549/DTX tumor xenograft models under specific pathogen-free conditions. Mice were housed in a room at a constant temperature (ca. 24 ± 1 °C) and humidity (ca. 60% ± 2%) with 12-h light/dark cycles. All mice were allowed free access to chow and water. All animal experimental procedures were approved by the Animal Ethics Committee of China Pharmaceutical University (30/04/2020, reference number: 2020-PKPD-04-30) and performed in accordance with the US National Institutes of Health guidelines. Approximately 5×10^6 A549 or A549/DTX cells were injected into the axilla of nude mice.

(1) Comparison of drug efficacy between sensitive and resistant tumor-bearing mice

When tumor volumes were greater than 80 mm³, xenograft mice were randomly assigned to carry out the experiment. The A549 and A549/DTX xenograft mice were allocated into four groups: the A549 vehicle (SC), A549 DTX (SD), A549/DTX vehicle (RC), and A549/DTX DTX (RD) groups. The animals in the DTX groups were treated with intraperitoneal injection of DTX (8 mg/kg) every 4 d. The vehicle groups were given the corresponding solvent at the same time.

(2) Effect of cystine supplementation on A549/DTX tumor-bearing mice

When tumor volumes were greater than 100 mm³, xenograft mice were randomly assigned before the experiment was performed. A549/DTX xenograft mice were randomly assigned to four groups ($n = 8$ per group): the vehicle (tumor model), cystine (60 mg/kg cystine intraperitoneally injected every day), DTX (8 mg/kg DTX, intraperitoneally injected every 4 d), and DTX + cystine (60 mg/kg cystine intraperitoneally injected every day plus 8 mg/kg DTX intraperitoneally injected every 4 d) groups. In addition, there was a control group of tumor-free mice. The control, vehicle, cystine and DTX groups were given the corresponding solvent at the same time. The length and width of the tumors and the body weight of the animals were recorded every 2–3 d.

On the last day of the experiment, the mice were sacrificed under anesthesia by intraperitoneal injection of avertin (7.2 mg/20 g body weight). Blood samples were collected into heparinized tubes via the retro-orbital sinus and centrifuged to obtain plasma. The plasma and tissues were stored at −80 °C until use for analysis.

Statistics
All the data are presented as the mean ± SEM. An unpaired *t* test with equal variance and one-way or two-way ANOVA followed by Bonferroni's multiple comparison test were used for statistical analyses. Statistical data analysis was performed using GraphPad Prism 6. Differences were considered significant at *,#$P < 0.05$; **,##$P < 0.01$; and ***,###$P < 0.001$.

RESULTS
Differential responses of sensitive and resistant A549 cells to DTX
To mimic the transition of sensitive cells into resistant cells, the parental A549 cell line, i.e., DTX-sensitive cells, was exposed to low levels of DTX (2 nM and 10 nM) [25], while derived A549/DTX cells,

which were resistant to DTX, were treated with 2 nM or 10 nM DTX, and cell viability was unchanged (Fig. 1a). In the A549 cells, 2 nM and 10 nM DTX caused slight decreases in the growth rate to 90.93% and 69.57%, respectively. When exposed to at least a thousand-fold higher levels of DTX (2 μM and 50 μM), the A549/DTX cells exhibited notable growth inhibition effects, similar to those exhibited by the A549 cells, for which the relative growth rate declined to 91.50% with 2 μM DTX treatment and to 73.55% with 50 μM DTX treatment for 24 h (Fig. 1a). A flow cytometric apoptosis assay showed that the high dose of DTX (10 nM) but not the 2 nM DTX dose was able to trigger significant apoptosis in A549 cells compared to control cells, and for A549/DTX cells, evident apoptosis was observed following cell exposure to fairly high concentrations of DTX (Fig. 1b). Statistically, 2 nM and 10 nM DTX resulted in increases in the apoptotic cell rate of 1.24- and 2.06-fold in the sensitive cells, respectively. The apoptosis rates of the A549/DTX cells incubated with 2 μM and 50 μM DTX were 2.63- and 4.04-fold higher than that of the control cells (Fig. 1b). The ability of the 10 nM DTX treatment to induce apoptosis in A549 cells was not significantly different from that of the 2 μM DTX treatment (a 200-fold higher concentration) in A549/DTX cells, which verified the resistance traits of A549/DTX cells.

The accumulation of DTX was further assessed by detecting its intracellular concentration with an LC-MS/MS assay. The content of intracellular DTX in the two cell lines generally increased as the concentration of DTX in the culture medium increased. After incubation for 24 h, the drug accumulation in the sensitive cells (0.292 ± 0.040 (2 nM), 1.022 ± 0.163 (10 nM) and 1.688 ± 0.124 (50 nM) nmol per mg of protein) was at least seven-fold higher than that in the resistant cells (0.040 ± 0.003 (2 nM), 0.102 ± 0.004 (10 nM) and 0.165 ± 0.018 (50 nM) nmol per mg of protein) at the same concentration (Fig. 1c). It is well documented that altered cellular pharmacokinetics, especially decreased intracellular drug accumulation, result from active excretion of chemotherapeutic drugs by the overexpression of efflux pumps, such as P-gp. As previously reported, the gene expression level of P-gp in A549/DTX cells was 406.639-fold higher than that in sensitive cells ($P = 0.00026$, Fig. 1d). The protein level of P-gp in A549/DTX cells was also higher than that in A549 cells (Fig. 1e and 1f). Moreover, flow cytometric analysis of intracellular Rho123 showed that the function of P-gp in A549/DTX cells was stronger than that in A549 cells, as indicated by the increased efflux of Rho123 (Fig. 1g).

Collectively, these data suggest that A549 and A549/DTX cells represent DTX-sensitive and DTX-resistant phenotypes, respectively, and that these cells show varied responses to DTX, as characterized by cell viability determination, apoptosis detection, drug accumulation analysis and drug transporter expression results.

The metabolic phenotype of resistant A549/DTX cells is characterized by increased oxidative stress and inhibited antioxidative potency
The intracellular and extracellular metabolites of A549 cells incubated either with or without DTX for 24 h were profiled using LC Q-TOF/MS and GC/MS, as were those of A549/DTX cells. The total ion current of a typical chromatogram showed that a large number of peaks were detected in the cell extracts and medium (Fig. S1). Deconvolution of the GC/MS chromatograms produced a total of 115 distinct peaks in the cell samples with 92 authentically identified metabolites, while in the medium samples, 70 metabolites were identified. In contrast, more metabolites (136 and 121 in the cells and medium, respectively) were detected by LC Q-TOF/MS, although some of these molecules overlapped with the metabolites identified by GC/MS (Table S2). Although the majority of the identified metabolites were shared between the cells and medium, some metabolites were exclusively detected in either the cells or the medium, as shown by the Venn diagram, which indicates the active substance exchange and metabolism of
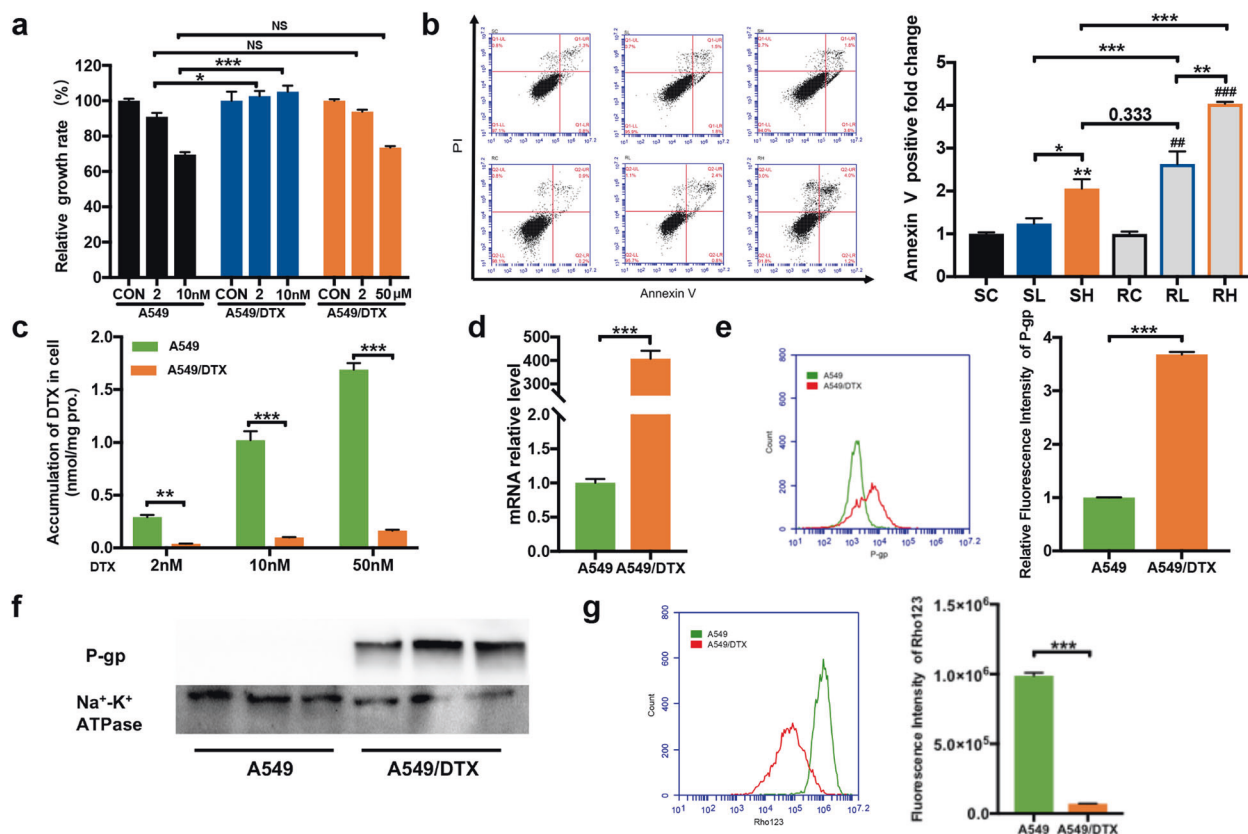
Supplementary cystine reverses the resistance of A549 cells
SJ Li et al.

2135

Fig. 1 Differential responses of sensitive and resistant A549 cells to DTX. a Viability of cells after incubation with DTX for 24 h, as measured with a CCK-8 assay ($n = 6$). **b** Apoptosis of cells after incubation with DTX for 24 h (SC: control A549 cells; SL: A549 cells+2nM DTX; SH: A549 cells+10nM DTX; RC: control A549/DTX cells; RL: A549/DTX cells+2 μM DTX; and RH: A549/DTX cells+50μM DTX) ($n = 3$). **c** Intracellular accumulation of DTX in A549 cells and A549/DTX cells for 24 h ($n = 4$). **d** mRNA levels of P-gp in A549 and A549/DTX cells ($n = 4$). **e** Immunofluorescence staining of P-gp expression in A549 and A549/DTX cells ($n = 4$). **f** Protein levels of P-gp in A549 and A549/DTX cells. The experiments were performed three times with similar results. **g** Fluorescence intensity of Rho123 in A549 and A549/DTX cells ($n = 4$). Unpaired t test with equal variance or two-way ANOVA followed by Bonferroni's multiple comparison test. $*P < 0.05$; $**$, $^{##}P < 0.01$; $***$, $^{###}P < 0.001$; and NS, no significance. Data represent the mean ± SEM.

these cells (Fig. S2a). A supervised PLS-DA model was created with the samples designated into six groups. The two cell lines clustered within each group and were clearly separated from each other, indicating the different metabolic phenotypes of the sensitive A549 cells and the resistant A549/DTX cells (Fig. 2a). Similar to intracellular metabolism, the medium metabolic shift caused by DTX could be observed more clearly based on the PLS-DA submodels (Fig. 2b).

Drug-resistant cells were originally derived from sensitive cells continuously exposed to and induced by low levels of DTX for 1 month. The resistant A549/DTX cells were metabolically stable and hence represented a reprogrammed metabolic phenotype different from the sensitive cells. The metabolic differences between the two types of cells suggested metabolic features associated with resistance. In total, 176 intracellular metabolites and 112 extracellular metabolites were significantly different between the A549 and A549/DTX cell lines. Based on volcano plots, the metabolites in both the cells and the medium changed to a large extent (Fig. 2c, 2d; Table S3a, S3b). Pathway analysis suggested that glutathione biosynthesis metabolism (glycine and serine metabolism and cysteine and methionine metabolism), glucose metabolism (glycolysis and PPP), and nucleotide metabolism (purine and pyrimidine metabolism) were closely related to DTX resistance in A549 cells (Fig. S2b–S2e).

Specifically, we found significantly higher levels of cystine, cysteine, GSH and GSSG in the sensitive cells than in the resistant

cells, while the level of extracellular cystine was much lower for the sensitive cells than for the resistant cells, indicating that the sensitive A549 cells needed and utilized more cystine, while the resistant A549 cells relied on cystine to aconsiderably reduced extent (Fig. 3a). In addition, compared with the levels in the sensitive cells, more methionine and serine accumulated in the drug-resistant cells but less accumulated in the medium, while intracellular and extracellular homocysteine levels were significantly increased. To our surprise, both the intracellular and extracellular levels of the key downstream metabolite cystathionine were much lower in the resistant cells.

To evaluate the heavily involved pathways, the key transporters and enzymes involved in the disturbed pathways were analyzed by q-PCR and Western blotting. We detected a dramatically lower abundance of enzymes involved in the cystine cycle and glutathione biosynthesis, such as SLC7A11, γ-GCS, and GSS, in A549/DTX cells than in sensitive cells (Fig. 3b, 3c). The data confirmed that cystine in the medium was rapidly utilized by sensitive A549 cells, which exhibited high expression and activity of SLC7A11 compared with A549/DTX cells. The ratio of GSH/GSSG in resistant cells was significantly lower than that in sensitive cells (Fig. 3d). The basal ROS level of drug-resistant cells was approximately 4.86-fold higher than that of sensitive cells (Fig. 3e). These data suggested that drug-resistant A549/DTX cells had a metabolic phenotype of high oxidative stress and a low antioxidant stress capacity.
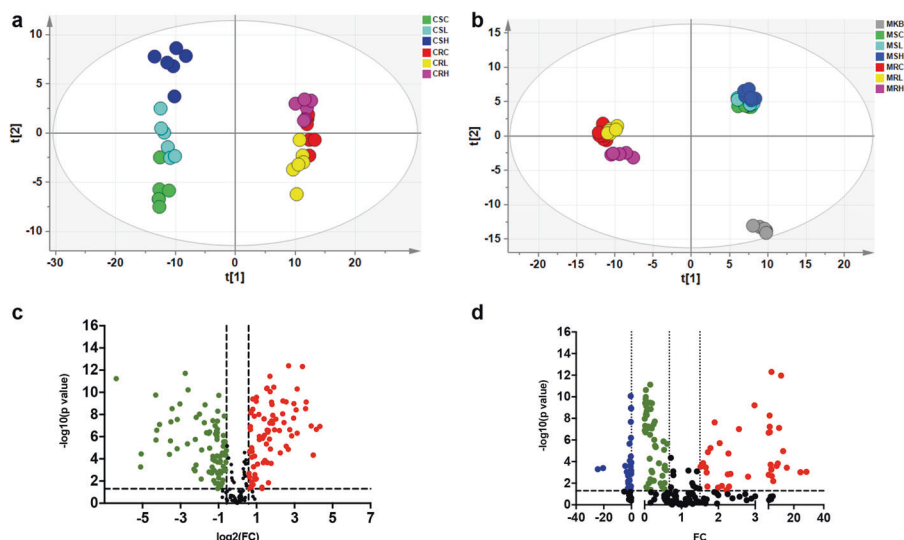
Supplementary cystine reverses the resistance of A549 cells
SJ Li et al.

2136

Fig. 2 Metabolic phenotypes of sensitive and resistant cells. a The PLS-DA model of cells (PC1: R^2X (cum) = 0.526, R^2Y (cum) = 0.199, Q2 (cum) = 0.187; PC2: R^2X (cum) = 0.603, R^2Y (cum) = 0.374, Q2 (cum) = 0.307; all 6 PCs: R^2X (cum) = 0.838, R^2Y (cum) = 0.965, Q2 (cum) = 0.787) (CSC: control A549 cells; CSL: A549 cells+2 nM DTX; CSH: A549 cells+10 nM DTX; CRC: control A549/DTX cells; CRL: A549/DTX cells+2 μM DTX and CRH: A549/DTX cells+50 μM DTX). **b** The PLS-DA model of the medium (PC1: R^2X (cum) = 0.396, R^2Y (cum) = 0.166, Q2 (cum) = 0.153; PC2: R^2X (cum) = 0.582, R^2Y (cum) = 0.332, Q2 (cum) = 0.317; all 6 PCs: R^2X (cum) = 0.75, R^2Y (cum) = 0.685, Q2 (cum) = 0.569) (MKB: original culture medium; MSC: medium from control A549 cells; MSL: medium from A549 cells+2 nM DTX; MSH: medium from A549 cells+10 nM DTX; MRC: medium from control A549/DTX cells; MRL: medium from A549/DTX cells+2 μM DTX; MRH: medium from A549/DTX cells+50 μM DTX). **c** Metabolite volcano plot of the CSC group versus the CRC group. The red dots represent metabolites with a P value < 0.05 and fold change>1.50, the green dots represent metabolites with a P value < 0.05 and fold change < 0.67, and the black dots represent nonsignificant metabolites ($P > 0.05$). In addition, see Supplementary Table S3a for the corresponding statistical analysis. **d** Metabolite volcano plot of the uptake or efflux of metabolites in the medium. For extracellular metabolites, the amount of a substance in the original culture medium (MKB) was deducted from the measured value, and the extracellular metabolites were compared by their uptake or efflux at the same protein level. The red dots represent the uptake or excretion of metabolites with a P value < 0.05 and fold change>1.50, the green dots represent the uptake or excretion of metabolites with a P value < 0.05 and fold change < 0.67, the blue dots represent the reverse metabolite uptake and efflux with a fold change < 0, and the black dots represent nonsignificant metabolites ($P > 0.05$). In addition, see Supplementary Table S3b for the corresponding statistical analysis.

DTX reprogrammed sensitive cells to exhibit a metabolic phenotype similar to that of resistant cells

Moreover, DTX treatment disturbed the metabolites of resistant A549/DTX cells and their parental A549 cells to varying degrees (Fig. S3). By comparing the metabolites differentially perturbed by DTX, the levels of 11 metabolites were significantly changed in sensitive cells exposed to very low levels of DTX but not in resistant cells treated with much higher levels of DTX, and these 11 metabolites were thus identified as potential metabolic markers of DTX resistance (Table 1). Interestingly, cystine was particularly prominent among these differentially expressed metabolites, and pathway analysis showed that cystine-related metabolic pathways, such as cystine and methionine metabolism and glutathione metabolism, were heavily involved in DTX resistance (Fig. S2b–S2e). In general, DTX reduced intracellular cystine levels in a dose-dependent manner in sensitive A549 cells, and the expression of SLC7A11 was also downregulated (Fig. 3b, 3c). DTX also significantly decreased NADPH levels and increased GSSG levels in sensitive cells, revealing a redox status similar to that of resistant cells (Fig. 3a). When A549 cells were treated with different doses of DTX, the intracellular GSH/GSSG ratio decreased to varying degrees in a dose-dependent manner (Fig. 3d). In sensitive cells, the gene and protein expression of key enzymes in the GSH synthesis pathway, γ-GCS and GSS, were inhibited by DTX (Fig. 3b, 3c). In addition, DTX induced increases in ROS levels in the sensitive cells (Fig. 3e) and significantly elevated P-gp mRNA expression in a dose-dependent manner (Fig. 3f). These results indicated that DTX reprogrammed the metabolic phenotype, especially the redox state, of sensitive cells to be similar to that of resistant cells, mainly by inhibiting cystine uptake and GSH synthesis, and DTX treatment gradually induced the acquisition of typical drug-resistant properties, such as P-gp overexpression.

Imbalance in the oxidative stress microenvironment stimulated the occurrence and development of drug resistance

To verify the effect of ROS on the development of drug resistance, both A549 cells and A549/DTX cells were exposed to the ROS-inducing agent Rosup. Rosup induced the production of a large amount of ROS in a dose-dependent manner, which was reversed by NAC (a ROS scavenger) and cystine (Fig. 4a, 4b). As the dose of Rosup was increased, the accumulation of DTX in cells gradually decreased, and supplementation with cystine or NAC increased the uptake of DTX (Fig. 4c, 4d). The mRNA and protein expression of P-gp was upregulated with the increase in ROS levels, which was also reversed by NAC and cystine (Fig. 4e–4h). In addition, the generation of ROS enhanced the function of P-gp in a dose-dependent manner, as manifested by increased Rho123 efflux (Fig. 4i, 4j).

These data suggested that in either sensitive cells or resistant cells, increased oxidative stress stimulated the expression and function of P-gp and thus promoted the development of drug resistance. Scavenging ROS with NAC or cystine downregulated the P-gp overexpression caused by oxidative stress and reduced drug efflux, which was expected to partially reverse chemotherapy resistance. Moreover, it could be inferred that cystine supplementation might remodel oxidative stress and enhance the effect of DTX, responses that might be involved in the decrease in oxidative stress-induced P-gp overexpression.
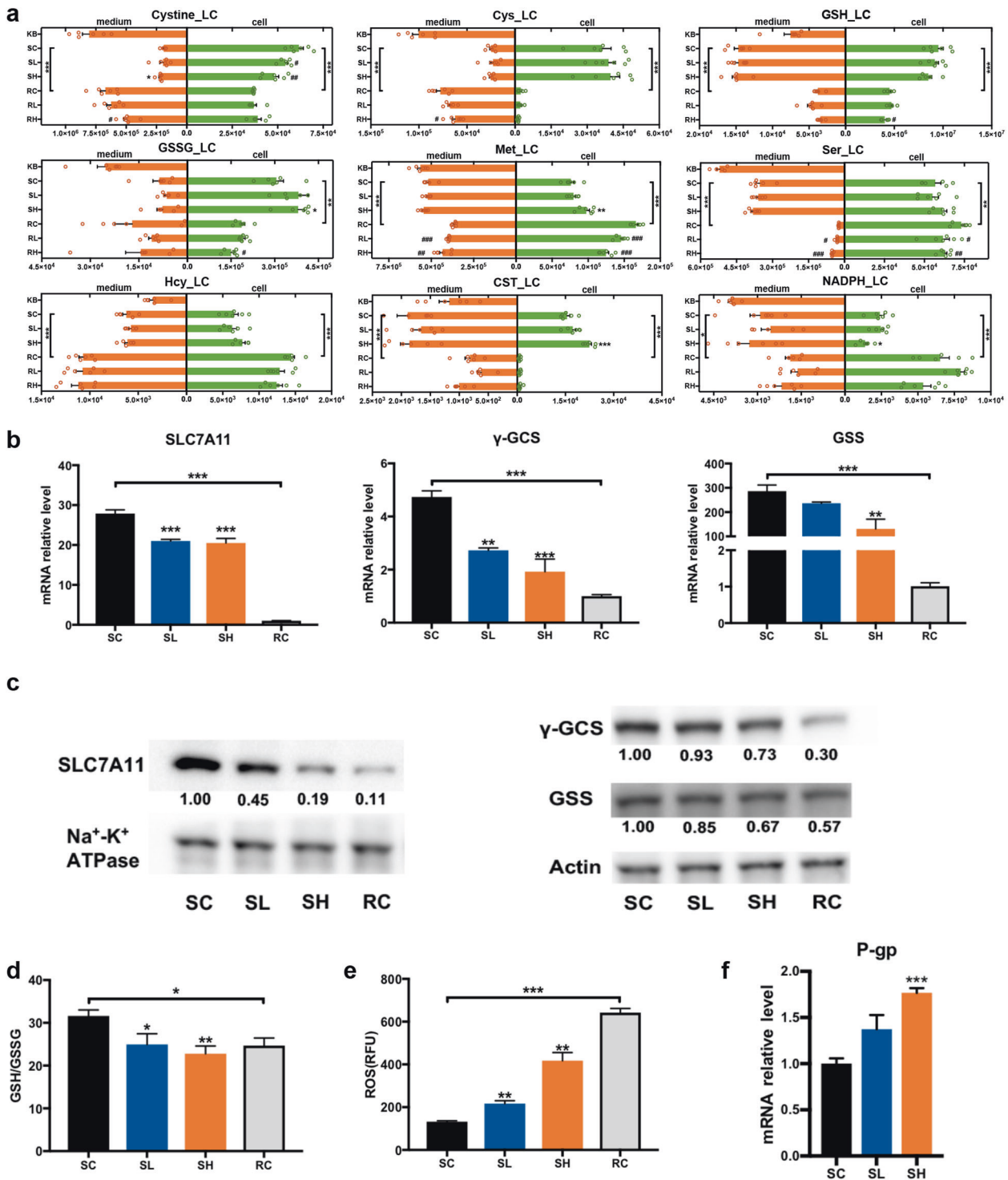
Supplementary cystine reverses the resistance of A549 cells
SJ Li et al.

2137

Fig. 3 The metabolic phenotype of resistant A549/DTX cells is characterized by increased oxidative stress and inhibited antioxidative potency. **a** Typical metabolic effects of DTX on the methionine cycle-transsulfuration-GSH pathway that impact the relative abundances of intracellular and culture medium metabolites from A549 cells and A549/DTX cells ($n = 6$) (KB: original culture medium; SC: control A549 cells; SL: A549 cells+2 nM DTX; SH: A549 cells+10 nM DTX; RC: control A549/DTX cells; RL: A549/DTX cells+2 μM DTX; RH: A549/DTX cells+50μM DTX). **b** mRNA levels of key enzymes in the cystine uptake-GSH synthesis pathway in A549 and A549/DTX cells treated with or without DTX for 24 h ($n = 3$). **c** Protein levels of key enzymes in the cystine uptake-GSH synthesis pathway in A549 and A549/DTX cells treated with or without DTX for 24 h. The experiments were performed three times with similar results. **d** GSH/GSSG ratio in A549 cells and A549/DTX cells treated with or without DTX for 24 h ($n = 6$). **e** ROS levels in A549 and A549/DTX cells treated with or without DTX for 24 h ($n = 3$). **f** mRNA levels of P-gp in A549 cells treated with DTX for 24 h ($n = 3$). Unpaired t test with equal variance or one-way ANOVA followed by Bonferroni's multiple comparison test. *$P < 0.05$; **$P < 0.01$; ***$P < 0.001$. Data represent the mean ± SEM.

Supplementary cystine reverses the resistance of A549 cells
SJ Li et al.

2138

Table 1. The potential DTX-resistant markers.

	A549 (2 nM)		A549 (10 nM)		A549/DTX (2 μM)		A549/DTX (50 μM)	
	FC	P	FC	P	FC	P	FC	P
cystine	0.879	0.02137	0.779	0.00299	1.002	0.97115	1.064	0.24528
Trp	1.179	0.00313	1.521	0.00001	0.951	0.14048	0.993	0.82357
cAMP	0.854	0.01253	0.831	0.03036	1.177	0.07785	0.907	0.39345
Xanthosine	2.041	0.01280	3.814	0.00033	0.641	0.05243	0.884	0.24973
ATP	0.811	0.00218	0.761	0.00231	0.905	0.21621	1.029	0.69471
UTP	0.679	0.00013	0.658	0.00055	1.097	0.32369	1.070	0.35127
HMG-CoA	0.616	0.01557	0.563	0.01414	0.964	0.84965	1.137	0.57480
Suc-CoA	0.678	0.00146	0.685	0.01314	0.906	0.56102	0.922	0.58716
Glucosamine-1P	1.439	0.01124	1.671	0.00702	0.928	0.26694	1.003	0.96883
TMP	5.221	0.00498	9.361	0.00027	0.879	0.37417	1.100	0.38362
CST	1.115	0.19337	1.448	0.00009	1.082	0.71889	1.195	0.55445

Cystine supplementation enhanced the effect of DTX in vitro

To investigate the aforementioned inference, we first tested whether cystine supplementation can revert the metabolic phenotype, especially in an induced oxidative stress system. We were pleased to find that cystine supplementation reversed the metabolic phenotype of resistant cells to be similar to that of sensitive cells (Fig. 5a). As the primary source substrate for GSH synthesis, cystine scavenged ROS (Fig. 5b) and promoted intracellular GSH synthesis (Fig. 5c) after supplementation in A549/DTX cells. Cystine also stimulated the protein expression of γ-GCS and GSS, activated the GSH synthesis pathway, and improved the antioxidant ability of A549/DTX cells (Fig. 5d).

Cell viability assays indicated that cystine supplementation enhanced the inhibitory effect of DTX on A549/DTX cell proliferation, and the inhibition rates induced by DTX at 0.5 μM, 1 μM, 2 μM, 10 μM, 50 μM and 100 μM were increased by 1.74-, 1.91-, 1.80-, 2.06-, 1.77- and 1.57-fold, respectively (Fig. 5e). Cystine supplementation significantly promoted early apoptosis in A549/DTX cells triggered by DTX, in contrast to the effect of 10 μM DTX alone (Fig. 5f). Interestingly, the accumulation of intracellular DTX was significantly increased after 1.0 mM cystine was added to A549/DTX cells (Fig. 5g), as was the nuclear and cytosolic distribution of DTX (Fig. 5h). We found that DTX stimulated P-gp gene and protein overexpression, which was reversed by cystine supplementation (Fig. 5i, 5j). Consistent results were also found by immunofluorescence analyses, which suggested that DTX enhanced the function of P-gp and the efflux of Rho123 was reduced after the addition of cystine (Fig. 5k, 5l).

Similar to the effects on drug-resistant cells, supplemental cystine significantly balanced the redox microenvironment by eliminating ROS (Fig. S4a) and activating GSH synthesis (Fig. 5m). Cystine supplementation also reversed the high expression of P-gp caused by DTX treatment (Fig. 5n) and enhanced the effect of DTX on sensitive A549 cells (Fig. 5o). Consistent results were confirmed by drug accumulation and subcellular distribution analyses (Fig. S4b, S4c) and P-gp expression and functional analyses (Fig. S4d, S4e) in A549 cells.

These data suggest that rebalancing the redox microenvironment with cystine supplementation can not only enhance the effects of drugs, especially in resistant cells, but can also attenuate the upregulation of efflux transporters induced by chemotherapeutic drug stimulation, which will reduce the incidence of chemotherapeutic drug resistance.

Differential response to DTX and differential metabolic phenotypes in sensitive and resistant tumor-bearing mice

Tumor-bearing mouse models established with sensitive A549 cells or A549/DTX drug-resistant cells were validated. DTX significantly inhibited the growth of tumors generated by sensitive cells but did not affect that of tumors consisting of drug-resistant cells (Fig. 6a). In the PLS-DA diagram of tumor metabolomics, the distance between the vehicle group and the DTX group of sensitive cell-derived tumors was greater than that of drug-resistant cell-derived tumors, suggesting that DTX had a stronger effect on the metabolism of the sensitive cell tumors, in which it showed more obvious efficacy (Fig. 6b). The concentration of DTX in tumors in the sensitive model was 3.31-fold higher than that in tumors in the drug-resistant model (Fig. 6c), while the plasma concentration of DTX showed no significant differences among the mice with different types of tumors (Fig. 6d), which indicated that the differential distribution of DTX in tumor tissues contributed to the differences in DTX efficacy between the sensitive and resistant tumor models. Consistent with the in vitro results, the gene and protein levels of P-gp in the tumor tissues of the DTX-resistant model were higher than those in the tumor tissues of the sensitive model (Fig. 6e, 6f).

Moreover, we observed that the levels of cystine and GSH in tumors formed by inoculated A549/DTX cells were decreased compared to those in tumors derived from A549 cells (Fig. 6g). The protein expression levels of the two key enzymes in GSH synthesis in the drug-resistant tumors were lower than those in the sensitive tumors (Fig. 6h). The results indicated that resistant cells shared a similar microenvironment both in vivo and in vitro, which was different from that of sensitive tumors due to the reduced antioxidant capacity and higher P-gp expression in the former.

Cystine supplementation enhanced the effect of DTX on A549/DTX cells in vivo

The effect of cystine supplementation on the efficacy of DTX was further studied in established sensitive and resistant tumor-bearing mouse models. We observed that cystine effectively enhanced the antitumor effect of DTX (Fig. 7a). The inhibitory effect of combined application of cystine and DTX on tumor growth was significantly larger than that of DTX monotherapy in mice, as manifested by smaller tumor volumes and weights, with the tumor volume inhibition rate in the combined group being approximately 3.05-fold greater than the DTX monotherapy group (P = 0.021) (Fig. 7b, 7c). The q value of the combined drug index as determined by Jin's formula was 1.57, and the coefficient of drug

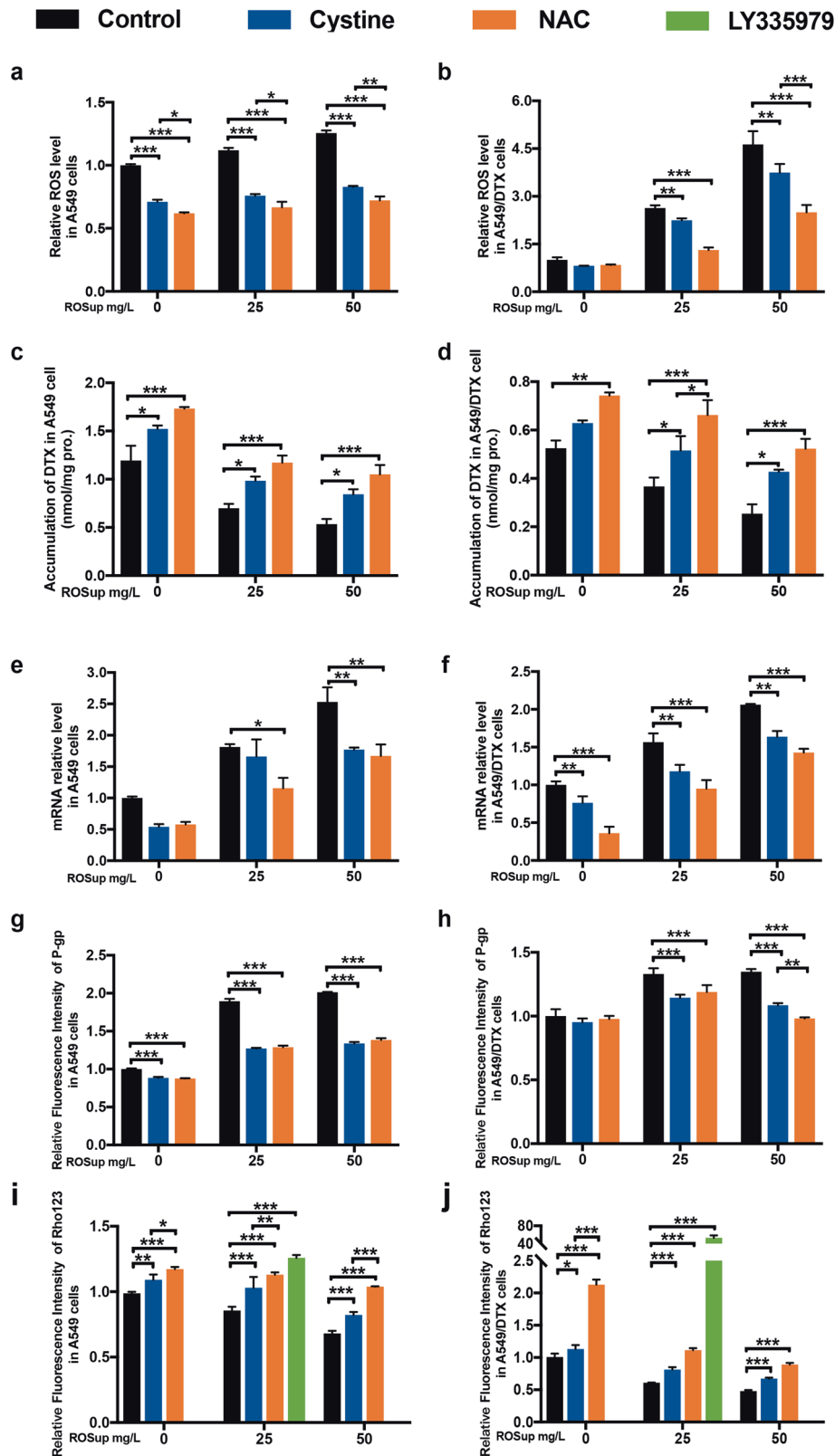Supplementary cystine reverses the resistance of A549 cells
SJ Li et al.

2139

Fig. 4 Imbalance in the oxidative stress microenvironment promoted the occurrence and development of drug resistance. a, b ROS levels in A549 (**a**) and A549/DTX cells (**b**) treated with Rosup or cystine or NAC supplementation for 12 h. Intracellular accumulation of DTX in A549 (**c**) and A549/DTX cells (**d**) treated with Rosup or cystine or NAC supplementation for 12 h. mRNA levels of P-gp in A549 (**e**) and A549/DTX cells (**f**) treated with Rosup or cystine or NAC supplementation for 12 h. Immunofluorescence staining of P-gp in A549 (**g**) and A549/DTX cells (**h**) treated with Rosup or cystine or NAC supplementation for 12 h. Fluorescence intensity of Rho123 in A549 (**i**) and A549/DTX cells (**j**) treated with Rosup or cystine or NAC supplementation for 12 h. Two-way ANOVA followed by Bonferroni's multiple comparison test. *$P < 0.05$; **$P < 0.01$; ***$P < 0.001$. Data represent the mean ± SEM, $n = 3$.

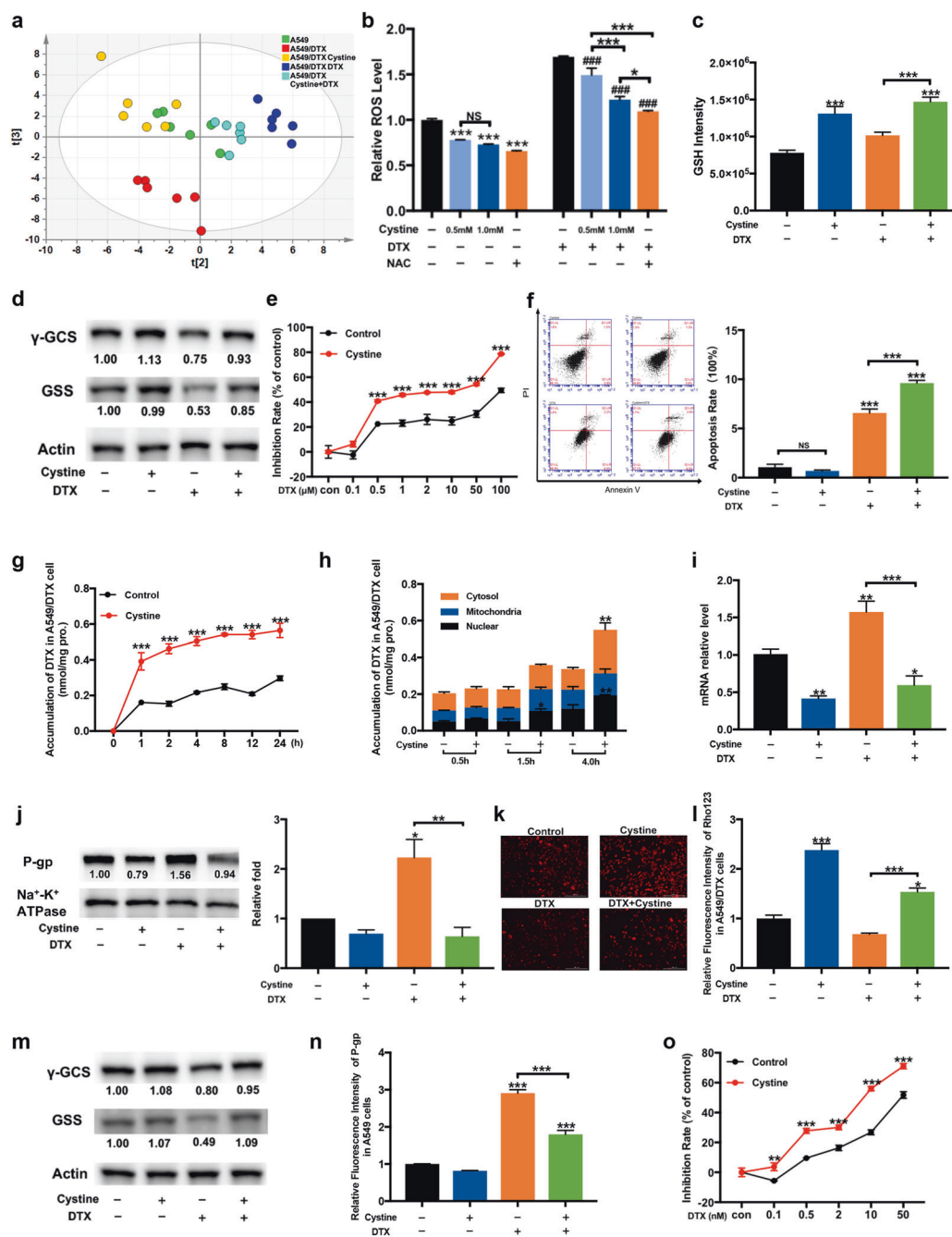Supplementary cystine reverses the resistance of A549 cells
SJ Li et al.

2140

Fig. 5 Supplementation with cystine enhanced the efficacy of DTX in vitro. a The PLS-DA model for A549/DTX cells given cystine supplementation for 48 h and A549 cells (PC1: R^2X (cum) = 0.447, R^2Y (cum) = 0.245, Q2 (cum) = 0.237; PC2: R^2X (cum) = 0.575, R^2Y (cum) = 0.457, Q2 (cum) = 0.375; PC3: R^2X (cum) = 0.700, R^2Y (cum) = 0.651, Q2 (cum) = 0.571) ($n = 6$). **b** Effect of cystine or NAC supplementation for 48 h on ROS levels in A549/DTX cells ($n = 3$). **c** Effect of cystine supplementation for 48 h on GSH levels in A549/DTX cells ($n = 6$). **d** Effect of cystine supplementation for 48 h on the protein levels of key enzymes in the GSH synthesis pathway in A549/DTX cells. The experiments were performed three times with similar results. **e** Effect of cystine supplementation for 48 h on the viability of A549/DTX cells ($n = 3$). **f** Sufficient cystine supplementation for 48 h affected the ability of DTX to induce apoptosis in A549/DTX cells ($n = 3$). **g** Effect of cystine supplementation on the intracellular accumulation of DTX in A549/DTX cells ($n = 4$). **h** Effect of cystine supplementation on the subcellular organelle distribution of DTX in A549/DTX cells ($n = 3$). **i** Effect of cystine supplementation for 48 h on the mRNA level of P-gp in A549/DTX cells ($n = 3$). **j** Effect of cystine supplementation for 48 h on the protein level of P-gp in A549/DTX cells. The experiments were performed three times with similar results. **k** Effect of cystine supplementation for 48 h on the fluorescence intensity of Rho123 in A549/DTX cells. Scale bars, 200 μm; ($n = 3$). **l** Effect of cystine supplementation for 48 h on the fluorescence intensity of Rho123 in A549/DTX cells, as quantitatively measured with flow cytometry analysis. ($n = 3$). **m** Effect of cystine supplementation for 48 h on the protein levels of key enzymes in the GSH synthesis pathway in A549 cells. The experiments were performed three times with similar results. **n** Effect of cystine supplementation for 48 h on the protein level of P-gp in A549 cells ($n = 5$). **o** Effect of cystine supplementation for 48 h on the viability of A549 cells ($n = 3$). Two-way ANOVA followed by Bonferroni's multiple comparison test. $*P < 0.05$; $**P < 0.01$; $***,^{###}P < 0.001$. Data represent the mean ± SEM.

Supplementary cystine reverses the resistance of A549 cells
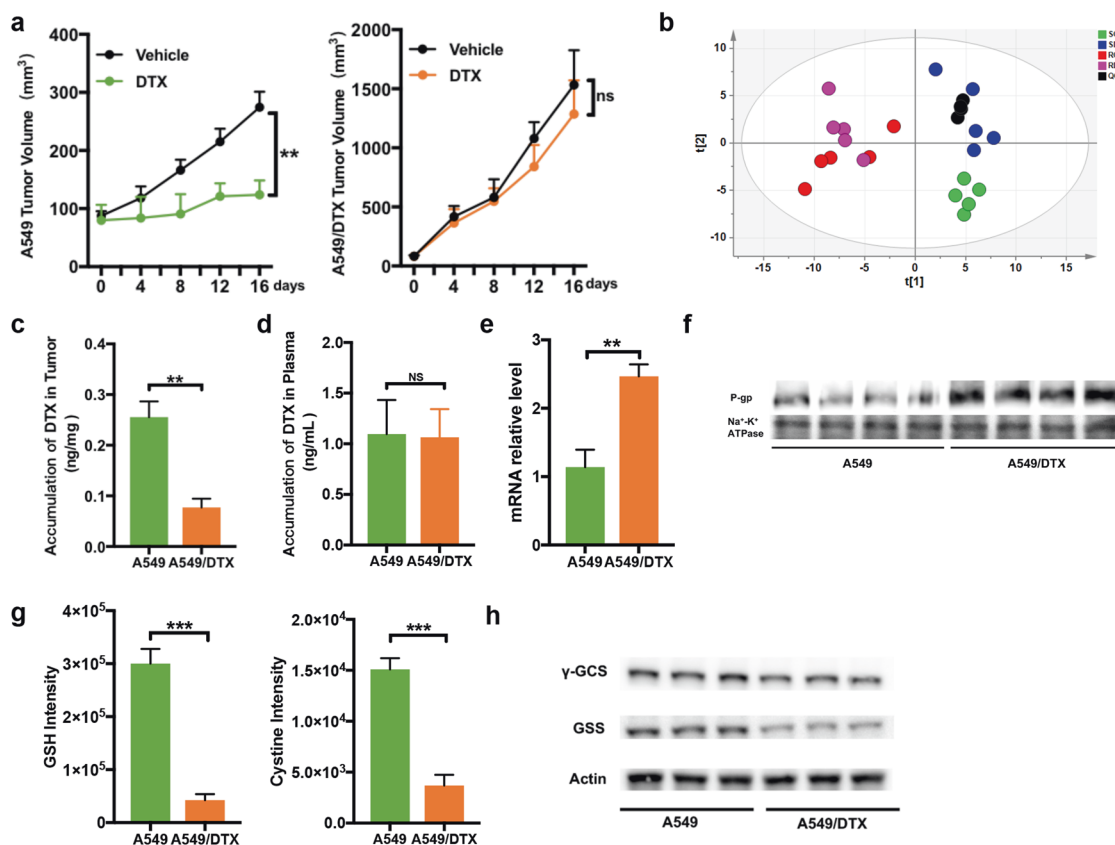SJ Li et al.

2141

Fig. 6 **Differential responses to DTX and differential metabolic phenotypes in sensitive and resistant cells. a** Mean tumor volumes on different days. Tumor volume was calculated as (length×width^2)/2. **b** The PLS-DA model of the tumors in different groups (SC:A549 tumor with vehicle treatment; SD: A549 tumor with DTX treatment; RC: A549/DTX tumor with vehicle treatment; RD: A549/DTX tumor with DTX treatment) (PC1: R^{2}X (cum) = 0.246, R^{2}Y (cum) = 0.23, Q2 (cum) = 0.171; PC2: R^{2}X (cum) = 0.365, R^{2}Y (cum) = 0.407, Q2 (cum) = 0.268). **c** Accumulation of DTX in A549 and A549/DTX tumors. **d** Accumulation of DTX in the plasma of A549 or A549/DTX tumor-bearing mice. **e** mRNA levels of P-gp in A549 and A549/DTX tumors. **f** Protein levels of P-gp in A549 and A549/DTX tumors. The experiments were performed three times with similar results. **g** GSH and cystine levels in A549 and A549/DTX tumors. **h** Protein levels of key enzymes in the GSH synthesis pathway in A549 and A549/DTX tumors. The experiments were performed three times with similar results. Unpaired t test with equal variance. *$P < 0.05$; **$P < 0.01$; ***$P < 0.001$. Data represent the mean ± SEM, $n = 5$.

interaction of the two drugs was 0.97, indicating DTX and cystine had synergistic effects. According to the PLS-DA diagram of the plasma metabolome, the metabolic phenotype of the cystine and DTX combined group deviated from that of the model group with successive changes causing the phenotype to become close to that of the normal group, suggesting that supplementation with cystine normalized the overall metabolism of tumor-bearing mice (Fig. 7d).

Cystine significantly increased the content of DTX in tumors by as much as 1.53-fold, leading to an improvement in the antitumor efficacy of DTX (Fig. 7e). Our data showed that the gene expression of P-gp in tumor tissue was elevated by 2.96-fold in the DTX group compared with the vehicle group but was significantly decreased by combined treatment with cystine (compared with the expression in the DTX group, $P = 0.000038$) (Fig. 7f). Cystine supplementation alone also reduced the mRNA level of P-gp in A549/DTX tumors. These results were further supported by the change in P-gp protein expression in tumors (Fig. 7g). We also observed an effect of cystine supplementation on redox homeostasis in A549/DTX tumor-bearing mice. The GSH level in the plasma of the tumor-bearing mice was significantly reduced compared with that in the plasma of the mice in the control group, and cystine supplementation increased the plasma GSH level with or without DTX administration (Fig. 7h). The supplemental cystine was distributed in the tumor, thereby

enhancing the antioxidative ability by promoting the synthesis of GSH (Fig. 7i, 7j). Cystine supplementation also increased the protein expression of γ-GCS and GSS, which was inhibited by DTX. Overall, cystine supplementation was beneficial in balancing microenvironmental redox homeostasis.

DISCUSSION
In the current study, the biological features and metabolic phenotypes of both DTX-sensitive cells and DTX-resistant cells were examined. Compared with the sensitive cells, the drug-resistant cells showed significantly different metabolic characteristics. The results showed that an imbalance in oxidative stress and metabolic changes were closely related to drug resistance. The genes critical for the cystine cycle and glutathione biosynthesis, such as SLC7A11, γ-GCS, and GSS, were markedly depressed in the resistant cells. The ratio of GSH/GSSG in the A549/DTX cells was lower than that in the A549 cells. Further experiments showed that DTX induced metabolic reprogramming in the sensitive cells, which subsequently exhibited metabolic characteristics similar to those of the drug-resistant cells. That is, the metabolism of the sensitive cells was reprogrammed by the change in the microenvironment, the imbalance in oxidative stress and the increased P-gp mRNA and protein levels. These findings strongly suggest that the influences of DTX on redox balance and the
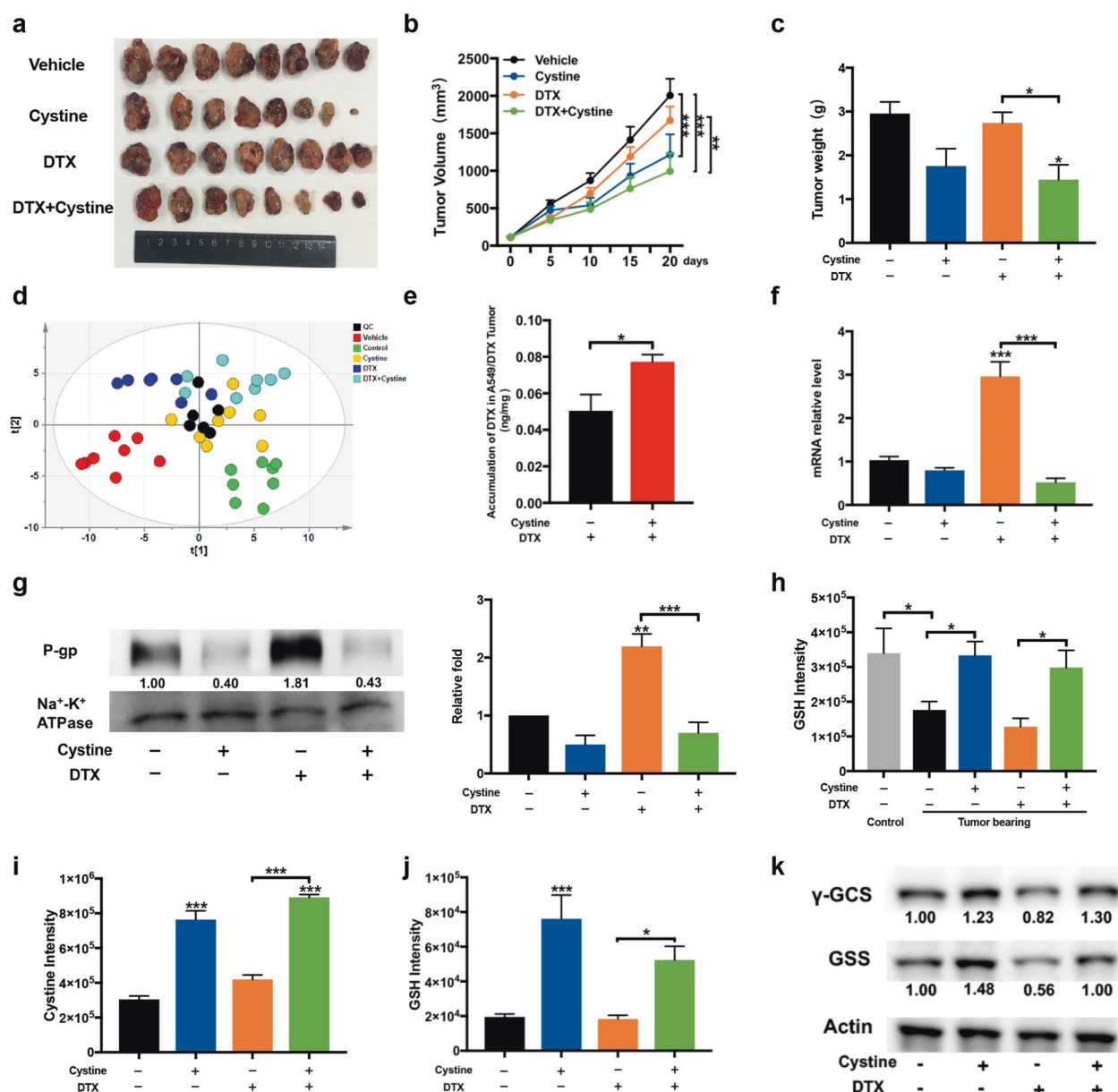
Supplementary cystine reverses the resistance of A549 cells
SJ Li et al.

2142

Fig. 7 Supplementation with cystine enhanced the efficacy of DTX in vivo. a Image of the tumors in different groups. **b** Mean tumor volumes on different days. Tumor volume was calculated as (length×width^2)/2 ($n = 8$). **c** Weights of the tumors in different groups ($n = 8$). **d** PLS-DA model of the plasma in the different groups (PC1: R^{2}X (cum)=0.178, R^{2}Y (cum) = 0.158, Q2 (cum) = 0.127; PC2: R^{2}X (cum) = 0.278, R^{2}Y (cum) = 0.331, Q2 (cum) = 0.265; all 3 PCs: R^{2}X (cum) = 0.361, R^{2}Y (cum) = 0.472, Q2 (cum) = 0.365) ($n = 8$). **e** Accumulation of DTX in A549/DTX tumors treated with or without cystine supplementation ($n = 6$). **f** mRNA levels of P-gp in A549/DTX tumors ($n = 6$). **g** Protein levels of P-gp in A549/DTX tumors ($n = 6$). **h** GSH levels in the plasma of A549/DTX tumor-bearing mice ($n = 8$). **i** GSH levels in A549/DTX tumors ($n = 6$). **j** Cystine levels in A549/DTX tumors ($n = 6$). **k** Protein levels of key enzymes in the GSH synthesis pathway in A549/DTX tumors. The experiments were performed three times with similar results. Unpaired t test with equal variance or two-way ANOVA followed by Bonferroni's multiple comparison test. *$P < 0.05$; **$P < 0.01$; ***$P < 0.001$. Data represent the mean ± SEM.

microenvironment are the cause of acquired drug resistance in A549 cells. An in-depth study showed that supplementation with NAC or cystine rebalanced redox homeostasis and reversed the aforementioned effects of DTX and cell resistance. This finding further indicates that the redox balance and changes in the microenvironment are the primary causes of resistance in A549 cells. Previous studies on the drug resistance of MCF-7 breast cancer cells showed that doxorubicin induced drug resistance in sensitive breast cancer cells, increased glycerol metabolism and ROS production, inhibited SLC7A11, reduced cellular uptake of cystine and inhibited GSH synthesis [18]. SLC7A11 overexpression,

cystine supplementation, ROS scavenging, and/or NAC addition can affect the redox balance of cells, significantly reduce the expression of P-gp, increase the uptake of doxorubicin and increase drug sensitivity or reverse drug resistance [19].

The similar changes in the microenvironment and drug resistance of the two cell lines strongly suggest that the drug resistance of tumor cells is closely related to oxidative stress imbalance, and there may be some common characteristics in tumor cell drug resistance. In addition, by providing cells with supplemental cystine, GSH synthesis and the antioxidative stress capacity of the cells can be significantly enhanced, which promotes

Supplementary cystine reverses the resistance of A549 cells
SJ Li et al.

2143

the efficacy of doxorubicin or DTX in vitro and in vivo and reduces drug resistance. It is suggested that cystine supplementation has important application value in reducing the expression and activity of P-gp and reversing drug resistance in tumor cells.

To verify the effects of cystine on GSH synthesis, ROS and P-gp levels, and adjuvant antitumor effects on resistant A549 cells, ideally, a comprehensive study should be conducted to assess the effects of cystine deprivation and sufficient cystine supplementation. Unfortunately, in in vivo experiments, cystine can not be removed from the diet, so verification of amino acid deprivation could not be carried out. Nevertheless, we unilaterally verified the consistency of the results in vitro and in vivo by cystine supplementation in tumor-bearing mice. Another alternative would be to inhibit SLC7A11 and limit the uptake and utilization of cystine by cells. However, no specific inhibitor of SLC7A11 without side effects is available. Although doxorubicin can strongly inhibit SLC7A11, it induces ROS production and P-gp expression and possesses antitumor effects [19]. Sulfadiazine is a potential inhibitor of SLC7A11. It is often used in the clinical treatment of inflammatory bowel disease and rheumatoid arthritis, has anti-inflammatory effects and affects the oxidative stress-related NF-κB and Nrf2 pathways [26–28]. Its potential capacity in the modulation of SLC7A11 needs to be further evaluated.

In conclusion, resistant A549 cells were characterized by reduced antioxidative potency. These cells utilized less cystine and synthesized less GSH than sensitive cells. Cystine supplementation increased GSH synthesis, altered the tumor microenvironment and redox homeostasis, reversed the overexpression of P-gp induced by DTX and enhanced the antitumor potency of DTX in vivo and in vitro. It is suggested that cystine supplementation is a potential strategy to enhance the effect of DTX on resistant tumor cells in the clinic.

AUTHOR CONTRIBUTIONS
JYA, SJL, BC, YX, and GJW designed the manuscript. SJL, ZYL, and SHG carried out the experiments. RBS, SJL, and ZYL analyzed the data. SJL and BC prepared the manuscript. JYA and GJW critically revised the manuscript.

ADDITIONAL INFORMATION
The online version contains supplementary material available at https://doi.org/10.1038/s41401-020-00610-3.

Competing interests: The authors declare no competing interests.

REFERENCES
1. Montero A, Fossella F, Hortobagyi G, Valero V. Docetaxel for treatment of solid tumours: a systematic review of clinical data. Lancet Oncol. 2005;6:229–39.
2. Fulton B, Spencer CM. Docetaxel. A review of its pharmacodynamic and pharmacokinetic properties and therapeutic efficacy in the management of metastatic breast cancer. Drugs. 1996;51:1075–92.
3. Herbst RS, Morgensztern D, Boshoff C. The biology and management of non-small cell lung cancer. Nature. 2018;553:446–54.
4. Chang A. Chemotherapy, chemoresistance and the changing treatment landscape for NSCLC. Lung Cancer. 2011;71:3–10.
5. Kim E. Chemotherapy resistance in lung cancer. Adv Exp Med Biol. 2016;893:189–209.
6. He XJ, Zhang TR. Alteration in the balance of prosurvival and proapoptotic signalling pathways leads to sequence-dependent synergism between docetaxel and sorafenib in human non-small cell lung cancer cell lines. Cell Biochem Biophys. 2014;68:411–8.
7. Chen HY, Shien K, Suzawa K, Tsukuda K, Tomida S, Sato H, et al. Elacridar, a third-generation ABCB1 inhibitor, overcomes resistance to docetaxel in non-small cell lung cancer. Oncol Lett. 2017;14:4349–54.
8. Kong WC, Ling XM, Chen Y, Wu XL, Zhao ZQ, Wang WW, et al. Hesperetin reverses P-glycoprotein-mediated cisplatin resistance in DDP-resistant human lung cancer cells via modulation of the nuclear factor-κB signaling pathway. Int J Mol Med. 2020;45:1213–24.
9. Hopper-Borge E, Chen ZS, Shchaveleva I, Belinsky MG, Kruh GD. Analysis of the drug resistance profile of multidrug resistance protein 7 (ABCC10): resistance to docetaxel. Cancer Res. 2004;64:4927–30.
10. Hanahan D, Weinberg R. Hallmarks of cancer: the next generation. Cell. 2011;144:646–74.
11. Tomita M, Kami K. Cancer. Systems biology, metabolomics, and cancer metabolism. Science. 2012;336:990.
12. Hiller K, Metallo M. Profiling metabolic networks to study cancer metabolism. Curr Opin Biotechnol. 2013;24:60–8.
13. Jain M, Nilsson R, Sharma S, Madhusudhan N, Kitami T, Souza A, et al. Metabolite profiling identifies a key role for glycine in rapid cancer cell proliferation. Science. 2012;336:1040–4.
14. Schulte M, Fu A, Zhao P, Li J, Geng L, Smith S, et al. Pharmacological blockade of ASCT2-dependent glutamine transport leads to antitumor efficacy in preclinical models. Nat Med. 2018;24:194–202.
15. Sullivan L, Luengo A, Danai LV, Bush LN, Diehl FF, Hosios AM, et al. Aspartate is an endogenous metabolic limitation for tumour growth. Nat Cell Biol. 2018;20:782–8.
16. Frezza C. Cancer metabolism: addicted to serine. Nat Chem Biol. 2016;12:389–90.
17. Pacold ME, Brimacombe KR, Chan SH, Rohde JM, Lewis CA, Swier LJ, et al. A PHGDH inhibitor reveals coordination of serine synthesis and one-carbon unit fate. Nat Chem Biol. 2016;12:452–8.
18. Cao B, Li MJ, Zha WB, Zhao QJ, Gu RR, Liu LS, et al. Metabolomic approach to evaluating adriamycin pharmacodynamics and resistance in breast cancer cells. Metabolomics. 2013;9:960–73.
19. Ge C, Cao B, Feng D, Zhou F, Zhang JW, Yang N, et al. The down-regulation of SLC7A11 enhances ROS induced P-gp over-expression and drug resistance in MCF-7 breast cancer cells. Sci Rep. 2017;7:3791.
20. Feng SQ, Wang GJ, Zhang JW, Xie Y, Sun RB, Fei F, et al. Combined treatment with apatinib and docetaxel in A549 xenograft mice and its cellular pharmacokinetic basis. Acta Pharmacol Sin. 2018;39:1670–80.
21. Wang WJ, Cai QY, Zhou F, Liu JL, Jin XL, Ni P, et al. Impaired pentose phosphate pathway in the development of 3D MCF-7 cells mediated intracellular redox disturbance and multi-cellular resistance without drug induction. Redox Biol. 2018;15:253–65.
22. Trygg J, Holmes E, Lundstedt T. Chemometrics in metabonomics. J Proteome Res. 2007;6:469–79.
23. Bjerrum JT. Metabonomics: analytical techniques and associated chemometrics at a glance. Methods Mol Biol. 2015;1277:1–14.
24. Xia J, Sinelnikov I, Han B, Wishart D. MetaboAnalyst 3.0–making metabolomics more meaningful. Nucleic Acids Res. 2015;43:W251–7.
25. Yang XL, Liu Y, Li WN, Li AM, Sun Q. DKK4-knockdown enhances chemosensitivity of A549/DTX cells to docetaxel. Acta Biochim Biophys Sin. 2017;49:899–906.
26. Gan HT, Chen YQ, Ouyang Q. Sulfasalazine inhibits activation of nuclear factor-kappaB in patients with ulcerative colitis. J Gastroenterol Hepatol. 2005;20:1016–24.
27. Kim JY, Cho H, Sir J, Kim B, Hur J, Youn S, et al. Sulfasalazine induces haem oxygenase-1 via ROS-dependent Nrf2 signalling, leading to control of neointimal hyperplasia. Cardiovasc Res. 2009;82:550–60.
28. Abbasi M, Mousavi M, Jamalzehi S, Alimohammadi R, Bezvan M, Mohammadi H, et al. Strategies toward rheumatoid arthritis therapy; the old and the new. J Cell Physiol. 2019;234:10018–31.